VIBRATION STUDY OF THE INTERMITTENT CONTROL FOR A SWITCHED RELUCTANCE MACHINE

Duy-Minh Nguyen, Imen Bahri, Guillaume Krebs, Éric Berthelot, Claude Marchand

VIBRATION STUDY OF THE INTERMITTENT CONTROL FOR A SWITCHED RELUCTANCE MACHINE

Duy-Minh Nguyen, Imen Bahri, Guillaume Krebs, Eric Berthelot, Claude Marchand

GeePs - Group of electrical engineering Paris, UMR CNRS 8507
CentraleSupélec, Univ. Paris-Sud, Univ. Paris-Saclay
Univ. Pierre et Marie Curie, Univ. Sorbonne
3, 11 rue Joliot-Curie, Plateau de Moulon 91192 Gif-sur-Yvette CEDEX, France
duy-minh.nguyen, claude.marchand@geeps.centralesupelec.fr

Abstract

The aim of the intermittent control (INC) is to increase the global efficiency of Switched Reluctance Machine (SRM) and its power converter in automotive applications. However, the SRM is characterized by vibro-acoustic noise which needs to be studied. This paper analyses the vibratory impact of the INC on the SRM and proposes a sliding strategy of this control to reduce such impact. This can be done rapidly in simulation by analyzing the radial forces, the deflections and the accelerations applied on the stator using a simplified electromagnetic-mechanical vibratory model of the SRM. The simulation results are then validated by experimental measures.

Keywords: switched reluctance machine, intermittent control, global efficiency, machine vibration, sliding control, simplified vibratory model, simulation, experimentation

1. INTRODUCTION

Nowadays, electric vehicles have become more popular thanks to their advantages such as high efficiency, low noise working and zero emission [1]. However, solutions that can extend the autonomy of the vehicles are still under interest. Besides, switched reluctance machines (SRM) are good candidates for traction engines in electric vehicles since they have low price, simple structure, high speed and high performance [2]. In the context of the electric vehicles and the SRM, previous papers investigated different losses of the SRM and their converters that influence the global efficiency of the system [3]-[5]. Then, some papers studied control strategies regarding efficiency criterion such as online commutation angle control [6] or impact of smooth torque control on efficiency [7]. In that context, the intermittent control (INC) has been proposed in [8] to firstly increase the global efficiency of the system comprising the SRM and its power converter by reducing the converter losses and the core losses. The INC is applied in medium-low torque zone of the torque-speed plane in both motor mode (green, positive torque) and generator mode (red, negative torque) where the driving cycles are distributed as shown in Fig. 1.

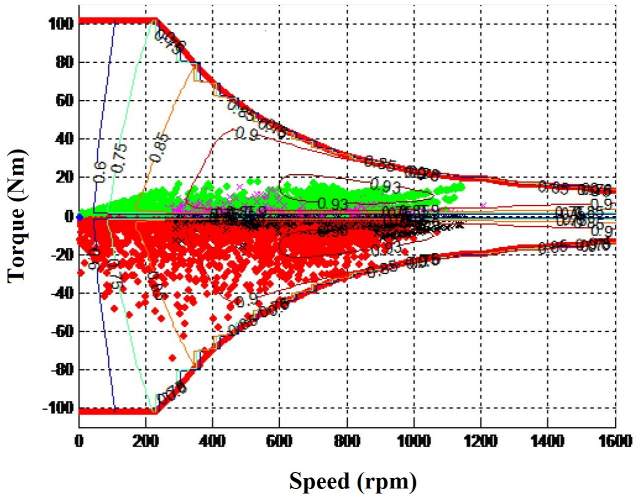

Figure 1: Solicitations of the electrical machine in electric vehicles on the driving cycle of French National Institute for Transport and Safety Research (INRETS) [9]

Nevertheless, the SRM is also known for vibro-acoustic noise mainly caused by stator vibration due to high radial force. Some papers study the vibro-acoustic phenomena of the SRM in [10], [11]. Others propose radial force controls in [12]-[13] to reduce the vibration. As a criterion in this paper, the vibratory impact of the INC is studied and a sliding strategy of the INC is proposed to reduce this impact. In fact, the electromagnetic radial force appears between the stator teeth and rotor teeth in operation. This force deforms periodically the stator structure, causing the vibration and the noise. At certain speeds, this force excites the natural frequencies of the stator that results in the resonance. This resonant vibration is particularly noisy. Thus, an accurate vibro-acoustic estimation of a SRM requires a complicated multi-physical model which takes not only time to develop but also time to simulate in finite element environment [14], [15]. In this paper, the authors use a simplified electromagnetic-mechanical vibratory model [16] to evaluate the vibratory impact of the INC. The vibratory impact of the INC is presented in [17] with simulation results. This model is simple and fast, while its accuracy is also validated by experimental results.

This paper has four parts. Section II describes the system before presenting the structure of the INC and its strategies. Section III presents the simplified electromagnetic-mechanical vibratory model for quick vibration evaluation. Section IV verifies the vibratory impact of the INC in simulation while section V validates these results in experimentation. Section VI concludes the vibratory impact of the INC and reveals the future works.

2. INTERMITTENT CONTROL

The studied system comprises an 8/6 four-phase double saliency SRM equipped with asymmetrical inverters. The nominal power is $1.2kW$. The maximal torque is $25Nm$. The nominal speed is $3000rpm$. This SRM is also used for experimental validations.

Table 1: System description

Characteristic	Value
Type	8/6 SRM, 4 phases
Nominal power	$1.2kW$
Maximal torque	$25Nm$
Nominal speed	$3000rpm$
Converter	Asymmetrical half bridge

The considered losses in the system are the converter losses (commutation and conduction ones) and the machine losses (core, winding, mechanical ones). The global efficiency η is calculated from the mechanical power P_{meca}, and the total loss P_{tot}.

$$\eta = \frac{P_{meca}}{P_{meca} + P_{tot}} \tag{1}$$

The INC aims to improve the global efficiency of the SRM and the converter in order to extend the autonomy of the vehicle. This control is based on the average torque control (ATC), which is featured for constant reference current over one conduction period. The ATC is studied in [18], [19] and applied from medium-high speed range where the SRM enters in the constant power region. The ATC structure (Fig. 2) comprises the speed regulation with an IP speed controller, the torque-current passage, and the current regulation with a hysteresis current controller. The conduction pulses generator computes the conduction pulses for the phases.

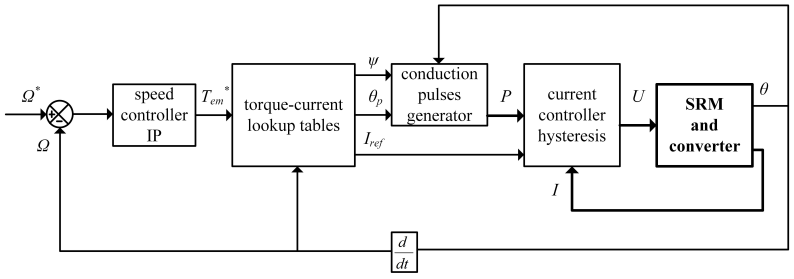

Figure 2: Structure of the ATC

The passage from the reference torque to the reference current, which is non-linear, is done by using the torque-current lookup tables. In the indirect average torque control, the phase torque is indirectly controlled through the phase current regulation which is characterized by three control parameters (control triplet) as illustrated in Fig. 3: current amplitude I_{ref}, turn-on angle ψ and conduction angle θ_p.

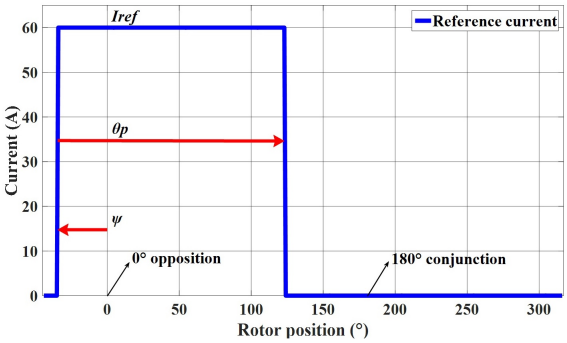

Figure 3: Three current control parameters

It is specified that the torque-current lookup tables are generated off-line from an optimal selection [20]. To operate the SRM at a specific torque-speed operating point, there are actually many possible control triplets. Only one control triplet is then selected to satisfy a control purpose such as minimization of torque ripple, minimization of machine vibration or maximization of global efficiency. In consideration of vehicle autonomy, the INC prioritizes the global efficiency of the system, thus the maximization of global efficiency criterion is chosen. Linear interpolation method is applied in on-line operation to computes the exact control triplet for various operating points.

Then, the principle of this control is deduced from the global efficiency map of the entire torque-speed plane (Fig. 4) given by the ATC. The system attends a global efficiency up to 77%. The maximum efficiency curve (MEC) is also plotted on this figure. The MEC traces the most efficient operating point at every speed. In other words, delivering this value of torque makes the system get the highest efficiency at the given speed.

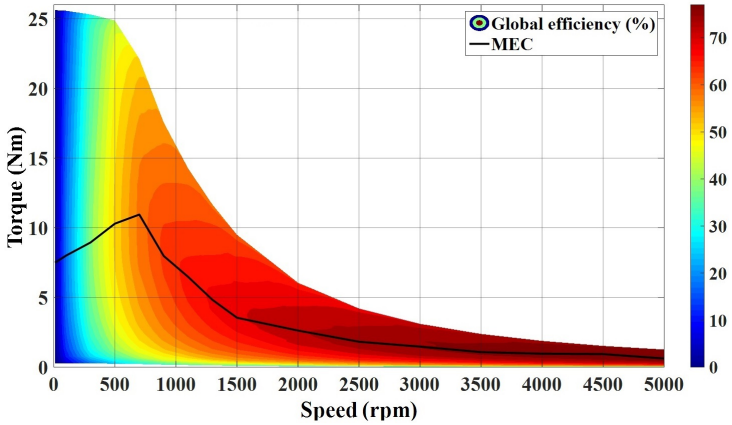

Figure 4: Global efficiency map with the MEC given by the ATC

Therefore, the idea of the INC is to bring each operating point under the MEC close to this curve by increasing the reference torque. At the same time, the average torque must be maintained as required by the speed controller. In order to do so, the paper [8] has presented the first approach involving in the electrical periods. In this approach, as this SRM has four phases, we can supply some phases with a higher reference torque while turn off the others during each electrical period to maintain the average torque as required.

2.1. INTERMITTENT CONTROL STRUCTURE

In order to realize the INC, the three blocks α-generator, torque adapter and pulse adapter are added to the ATC (Fig. 5, red).

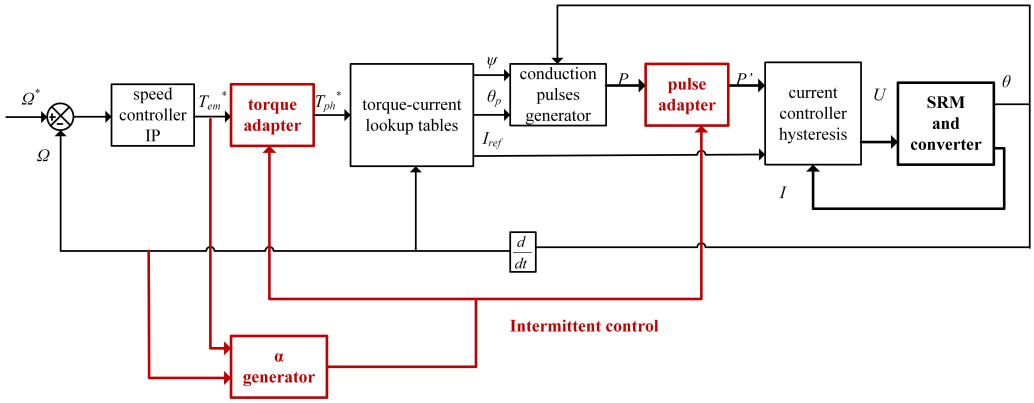

Figure 5: Structure of the INC

The INC is characterized by the duty cycle "α" which is the ratio between the number of supplied phase(s) k and the total number of phases q:

$$\alpha = \frac{k}{q}, \text{ where } 1 \leq k \leq q. \tag{2}$$

The α-generator is a duty cycle lookup table which is generated off-line from a selection algorithm. As defined in (2), there are four possible duty cycles 1/4, 2/4, 3/4, 4/4 (ATC) of the INC that can be applied for each operating point. First, only the duty cycles that let the machine operate within the torque-speed plane are permitted. Then, only one duty cycle that makes the system achieve the highest efficiency is selected. Nearest-neighbor interpolation method is applied in on-line operation.

Fig. 6 shows the obtained duty cycle lookup table of the INC. The duty cycles 1/4, 2/4, 3/4, 4/4 are respectively applied on zone (a), (b), (c) and (d) of the torque-speed plane. When the four phases are supplied ($\alpha = 4/4$), the INC works as the ATC since the system already achieves the highest efficiency. It is noted that the INC cannot be applied on the upper zone of the MEC.

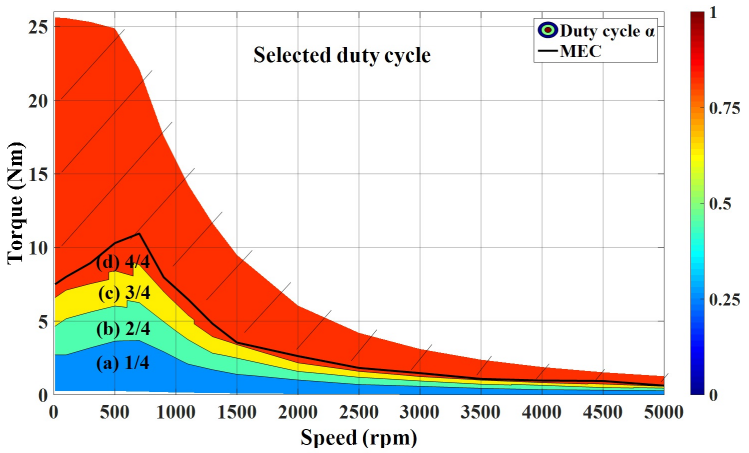

Figure 6: Duty cycle map of the INC

The torque adapter is a simple factor that calculates the reference torque T^*_{ph} of the supplied phase(s) from the required average torque T^*_{em} and the duty cycle α received from the α-generator:

$$\alpha.T^*_{ph} = T^*_{em}, \text{ thus } T^*_{ph} = \frac{1}{\alpha}.T^*_{em}. \tag{3}$$

The pulse adapter is an algorithm that decides which phase(s) to supply according to the duty cycle α received from the α-generator. Specifically, p_i is the conduction pulse of phase i by the ATC, $p_i^{'}$ is the conduction pulse of phase i by the INC and f_i is the phase-selection signal decided by the INC algorithm:

$$p_i^{'} = p_i.f_i, \text{ where } f_i = \begin{cases} 1, & \text{if phase i is ON} \\ 0, & \text{if phase i is OFF} \end{cases} \tag{4}$$

Different phase-selection strategies are presented in the next part. When the INC is activated, the α-generator computes the duty cycle α from the measured speed and the required torque. The duty cycle α is sent to both the torque adapter and the pulse adapter. At the same time, the torque adapter increases the reference torque while the pulse adapter turns off some phases.

Fig. 7 shows an example of the INC applied for the operating point speed $500rpm$, torque $6Nm$. The ATC (a) excites four phases with a reference torque of $6Nm$ and the efficiency achieves 57.62% (Fig. 4). The INC (b) excites two phases with a reference torque of $12Nm$ and the efficiency achieves 59.24%. The efficiency has been increased by 1.6% for the same average torque.

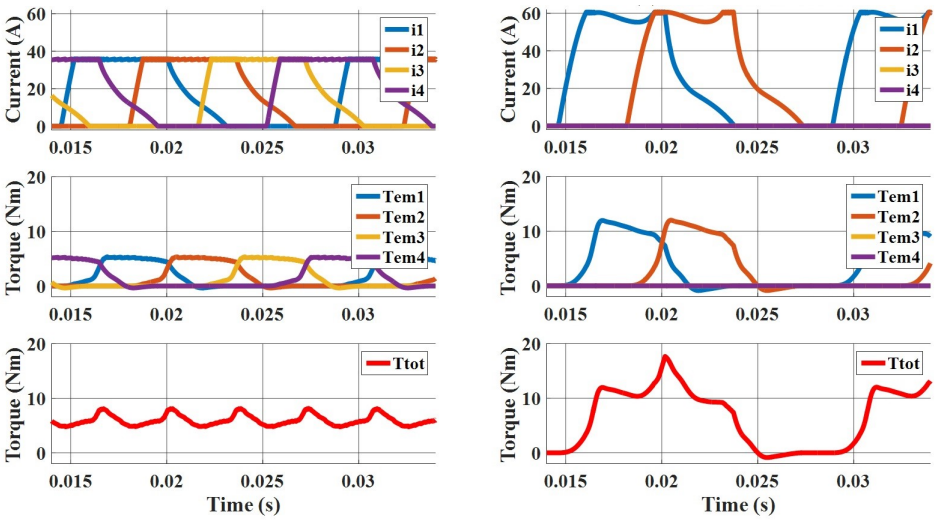

(a) ATC (b) INC

Figure 7: Current and torque waveforms at $500rpm$, $6Nm$, $\alpha = 2/4$

It is noticeable that the torque of the SRM given by the INC is even more rippled due to the increase of the reference torque and the turned off phases. In the example in Fig. 7, the torque ripple is increased from $3.2Nm$ (ATC) to $18Nm$ (INC) for the average torque of $6Nm$. Beside the vibration of the stator treated in this paper, this could also result in the vibration of the mechanical transmission system, causing uncomfortable vehicle jerks which is discussed in the paper [21].

2.2. INTERMITTENT CONTROL STRATEGIES

As the INC turns off some phases, one has the liberty to select among four phases which ones to supply. This part presents different phase-selection strategies of the INC which can influence the machine vibration [17] and the torque propulsion [21] generated by the SRM. In the initial strategy presented in the principle, the supplied phases are fixed in all electrical periods and there are six electrical periods (T_e) in each mechanical period (T_m). Now, the supplied phases are shifted regularly in the increasing direction (direct sliding). Fig. 8 shows the examples of the strategies where only one phase supplied with $\alpha = 1/4$.

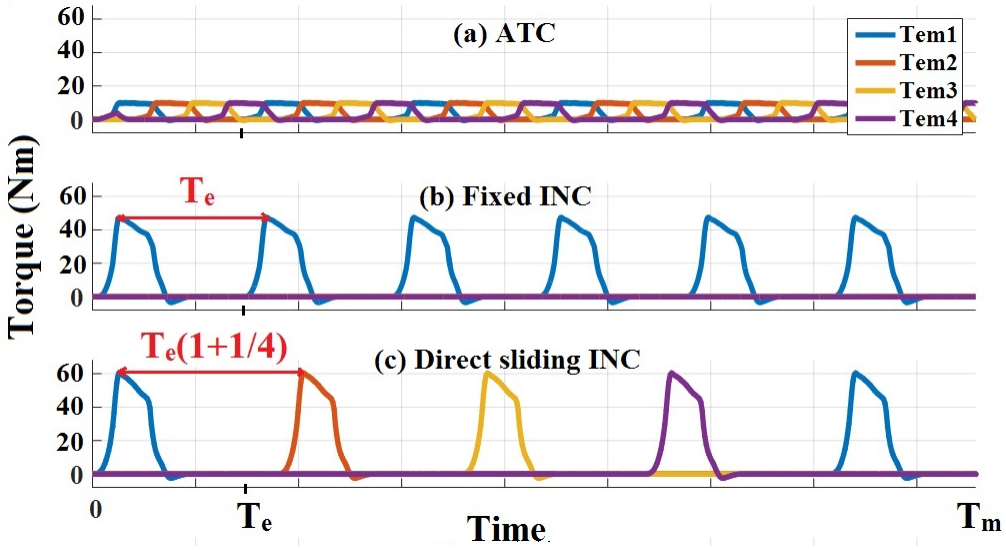

Figure 8: ATC and INC strategies at the operating point $500rpm$, $3Nm$, $\alpha = 1/4$

When the supplied phases are shifted regularly, the angular distance between two torque peaks changes. As a result, the number of torque peaks in each mechanical period changes, and the average torque is not assured anymore. Therefore, the reference torque needs to be compensated by a secondary factor called sliding cycle "β" calculated as the ratio between peak distance of the fixed strategy D_{fixed} and that of the sliding strategies $D_{sliding}$:

$$\beta = \frac{D_{fixed}}{D_{sliding}}. \tag{5}$$

The Eq. (3) becomes:

$$\alpha.\beta.T^*_{ph} = T^*_{em}, \text{ thus } T^*_{ph} = \frac{1}{\alpha}.\frac{1}{\beta}.T^*_{em}. \tag{6}$$

Fixed INC: the supplied phases, noted p_i, are fixed in all electrical periods (Fig. 8b). In this case, there are six torque peaks in each mechanical period, with $D_{fixed} = D_{sliding} = T_e$. The supplied phases are noted in Tab. 2.

Table 2: Fixed INC

α	**Supplied phase(s)**	β
1/4	p1	1
2/4	p1, p2	
3/4	p1, p2, p3	

Considering the energy aspect, the fixed INC can reduce the losses up to $30W$ in the applicable zone under the MEC as shown in Fig. 9.

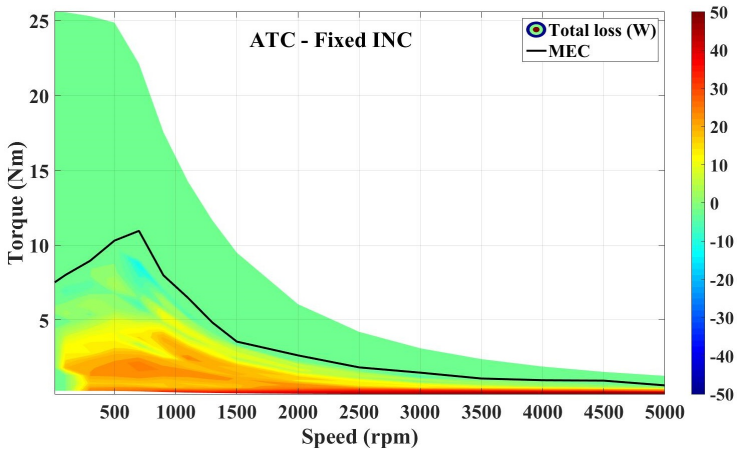

Figure 9: Total loss: ATC - Fixed INC

Direct sliding INC: the supplied phases are shifted regularly in the increasing direction (Fig. 8c). The peak distance $D_{sliding} = T_e(1 + 1/4)$ is higher. There are fewer torque peaks in each mechanical period. The generated frequencies of the currents and torques are lower, compared to the fixed strategy. As a result, the direct sliding INC improves the vibration of the SRM as demonstrated in [17]. The supplied phases are noted in Tab. 3.

Table 3: Direct sliding INC

α	**Supplied phase(s)**				β
1/4	p1	p2	p3	p4	4/5
2/4	p1, p2	p2, p3	p3, p4	p4, p1	
3/4	p1, p2, p3	p2, p3, p4	p3, p4, p1	p4, p1, p2	

In Fig. 10, this strategy still reduces the total losses up to $30W$ for the low torque zone (below $5Nm$), but the upper zone (between $5Nm$ and $10Nm$) is now negative due to the sliding cycle β which increases the reference torque beyond the maximum efficiency curve.

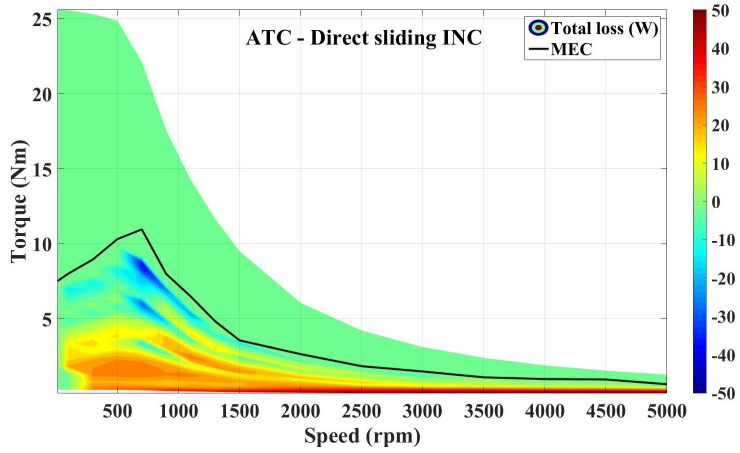

Figure 10: Total loss: ATC - Direct sliding INC

In the rest of the paper, authors propose to evaluate the vibratory impact of the fixed and direct sliding INC firstly by simulations using a simple vibratory model of the SRM and secondly by experimentations.

3. SIMPLIFIED VIBRATORY MODEL

The radial force is considered as the dominant force that deforms the stator. The radial force look-up table in terms of current and electrical position is given by a laboratory-made code based on finite elements analysis called MRVSIM [22].

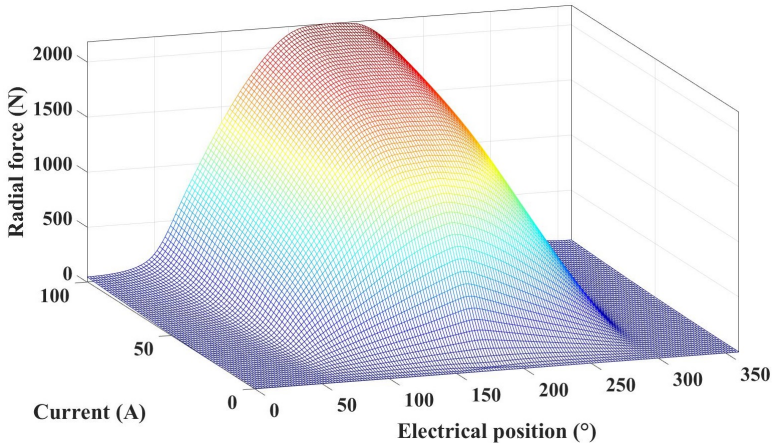

Figure 11: Radial force network versus phase current and electrical position

In rotation, the radial force is periodically applied on stator teeth and could excite the natural frequencies of the stator especially at certain speeds. This is the source of acoustic noise which needs to be mitigated. From a vibratory point of view, the SRM is a complicated multi-degree-of-freedom system which can be represented as a linear superposition of a finite number of single-degree-of-freedom systems [23]. In the acceleration calculation, the first step is to determine the main natural frequencies of the stator. These natural frequencies are obtained from modal analysis also with MRVSIM. The main vibratory Eigen modes of the stator structure are mode 2 ($2889Hz$), mode 3 ($7526Hz$), mode 4 ($12240Hz$, $12334Hz$, $14136Hz$) (Fig. 12).

It is noted that with the 8/6 SRM, the odd modes are not excited due to symmetrical excitation. Among the even modes, only the mode 2 is considered in this study as it is the most susceptible mode to be excited by the control strategies. Additionally, its frequency is closest to the fundamental frequency of the phase current. The advantage of the simplified vibratory model is that it allows fast verification of the vibratory impact of the INC on the entire speed range. The vibration mode 2 ($f_2 = 2889Hz$) of the stator is shown in Fig. 12. The blue areas represents the stator nodes with low deflection, while the yellow areas indicates high deflection.

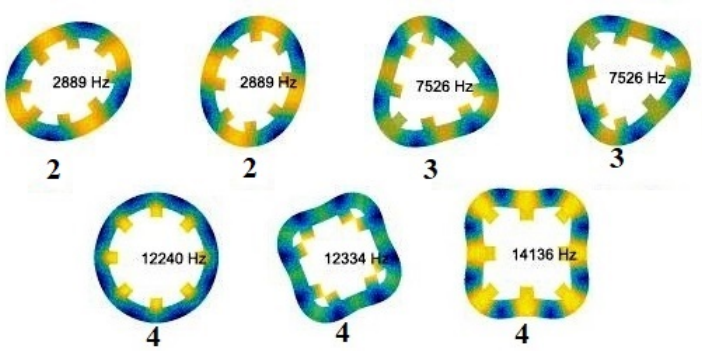

Figure 12: Vibratory modes of the stator

The behavior of the stator can be expressed as a mechanical spring-mass-damper system [24]. The relation between radial deflection $x(t)$, velocity $\dot{x}(t)$, acceleration $\ddot{x}(t)$ and the applied radial force $F(t)$:

$$M.\ddot{x}(t) + C.\dot{x}(t) + K.x(t) = F(t) \tag{7}$$

With M, C, K are respectively the local mass, the damping coefficient and spring constant of the system. The local mass M is the total mass of the iron core and the windings, divided by four. The values of the spring constant K and the damping coefficient C are calculated by:

$$K = M.\omega_n^2 \tag{8}$$

$$C = 2.M.\xi.\omega_n \tag{9}$$

Where ω_n is the natural pulsation and ξ is the damping coefficient which is experimentally identified in the way that the behavior of the vibratory model meets the actual behavior of the SRM's stator [16]. The numerical values of the model are written in Tab. 4.

Table 4: Factors of the spring-damper system

Factor	**Value**
Natural frequency f_2	$2889Hz$
Local mass M	$3kg$
Spring constant K	$9.98.10^8 N/m$
Damping coefficient C	$9.69.10^3 Ns/m$
Damping ratio ξ	0.089

Fig. 13 shows the Bode analysis of the spring-damper system. It is indicated that there is a resonance around of the vibration mode 2 of the stator which is $f_2 = 2889Hz$.

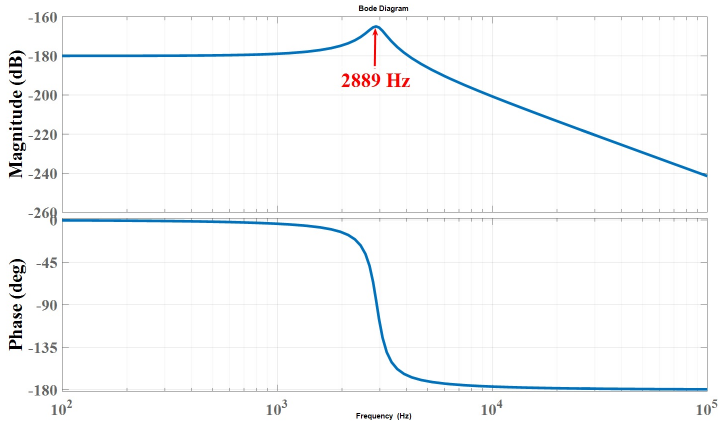

Figure 13: Bode diagram of the spring-damper system

From this bode diagram, the resonance at the mode 2 will happen when either the fundamental or a harmonic of the input radial force equals the resonant frequency f_2. In other words, certain rotor speeds will make the radial force contain f_2 and will excite the mode 2. The relation between the rotor speeds Ω (rpm) and the vibration mode f_2 (Hz) is explained in following equations.

The resonance condition is that the harmonic frequencies of the radial force f_f equals the resonant frequency f_2:

$$f_f = f_2 \tag{10}$$

Harmonics of the radial force f_f [25] is calculated from the mechanical frequency f_{meca}, where N_r is the number of rotor poles:

$$f_f = f_{meca}.N_r.n, \text{ where } n = 1, 2, 3... \tag{11}$$

Mechanical frequency f_{meca} is calculated from the rotor speed Ω:

$$f_{meca} = \frac{\Omega}{60} \tag{12}$$

Corresponding rotor speeds that excite the mode 2:

$$\Omega = \frac{f_2.60}{N_r.n} \tag{13}$$

Numerical values of the rotor speeds that excite the mode 2:

$$\Omega = \frac{28890}{n}(rpm) \tag{14}$$

In previous works [23], [24], Rasmussen has derived the vibratory calculation for switched reluctance machine, considering the mode n of the stator. This calculation is based on the wave propagation phenomenon on the stator surface.

The partial deflection at any pole j (x_{ji}) is propagated from the deflection source at phase i (x_{ii}). The deflection source itself is a function of time identified from the mechanical model (7).

$$x_{ji} = x_{ii}.\cos\left(\frac{2n\pi(j-i)}{N_s}\right) \tag{15}$$

Where N_s is the number of stator poles. The total deflection at the pole j (x_j) is the superposition of the partial deflections at pole j propagated from all the deflection sources, which are the excited phases.

$$x_j = \sum_{i=1}^{q} x_{ji} = \sum_{i=1}^{q} x_{ii}.\cos\left(\frac{2n\pi(j-i)}{N_s}\right) \tag{16}$$

The Eq. (16) is then expressed in matrix notation for a q-phase SRM. The matrix B of the coefficients is determined and implemented in simulation.

$$X_j = B.X_{ii}$$

$$\begin{bmatrix} x_1 \\ . \\ . \\ x_q \end{bmatrix} = \begin{bmatrix} b_{11} & . & . & b_{1q} \\ . & . & . & . \\ . & . & . & . \\ b_{q1} & . & . & b_{q4} \end{bmatrix} . \begin{bmatrix} x_{11} \\ . \\ . \\ x_{qq} \end{bmatrix} \tag{17}$$

$$\text{where } b_{ji} = \cos\left(\frac{2n\pi(j-i)}{N_s}\right)$$

The matrix B in (17) is written for the four-phase 8/6 SRM. It indicates that there are couplings between phase 1 and phase 3, as well as between phase 2 and phase 4.

$$B = \begin{bmatrix} 1 & 0 & -1 & 0 \\ 0 & 1 & 0 & -1 \\ -1 & 0 & 1 & 0 \\ 0 & -1 & 0 & 1 \end{bmatrix} \tag{18}$$

It is noted that similar equations can be defined for the radial velocity $\dot{x}$ and acceleration $\ddot{x}$. In brief, the vibratory computation comprises two steps. Firstly, the deflection or acceleration sources of the phases are obtained by the mechanical model in (7). Secondly, the total deflection or acceleration at any pole are computed by the matrix in (17).

4. SIMULATION VALIDATION

Fig. 14. shows an example of the input radial forces and the output deflections, accelerations given by the vibratory model. The operating point is $700rpm$, $6Nm$ with the direct sliding INC which supplies 3 phases.

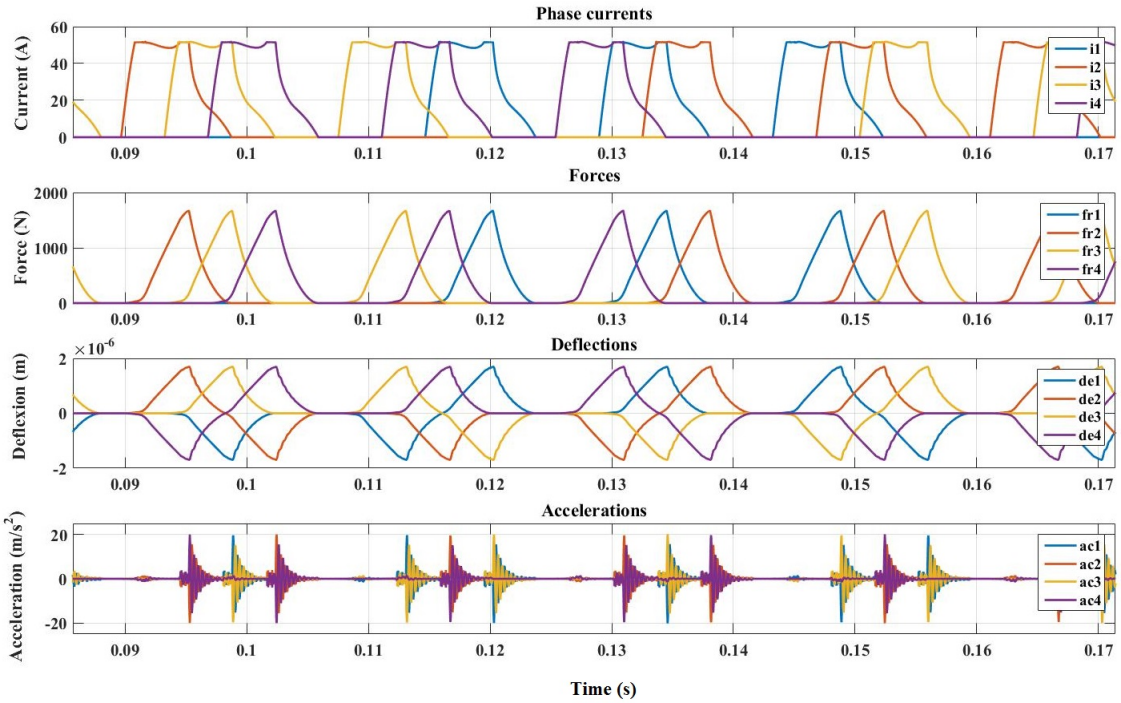

Figure 14: Current, force, deflection and acceleration waveforms given by the direct sliding INC at $700rpm$, $6Nm$ during one mechanical period

The spectrums of the radial forces, deflections and accelerations are analyzed. The energies of the accelerations are also considered. The local energy (E_{loc}) is the spectral energy within the resonance frequency range from $2400Hz$ to $3400Hz$ (Fig. 13), while the global one (E_{glo}) is the spectral energy of the audible frequency range from $20Hz$ to $20kHz$.

4.1. SPECTRAL ANALYSIS OF A SPECIFIC TORQUE-SPEED POINT

This analysis considers a specific operating point at $700rpm$, $6Nm$, where the fixed and the direct sliding strategies of the INC are applied with the duty cycle $\alpha = 3/4$ in comparison with the ATC.

First of all, the ATC excites four phases (Fig. 15a). The harmonic contents of the radial forces on each phase are identical and related to the rotational speed. The deflections and accelerations of four phases are given by the vibratory model in Eq. (7) and (17). The deflection peaks are identical and reach $0.25\mu m$ (Fig. 16a). The acceleration peaks are identical, equal to $0.5m/s^2$ and found at the mode 2 (Fig. 17a). The local and global energies of the accelerations are almost identical and equal to $9.7J$, $15.4J$ respectively on all phases.

The fixed INC excites only phases 1, 2 and 3 which have identical harmonic contents of the radial forces (Fig. 15b). The harmonic amplitudes of the radial forces in this case are slightly higher than those of the ATC due to the increase of the phase currents. Although only phase 1, 2 and 3 are excited, the deflections are found on all phases due to the wave propagation, or the couplings (Fig. 16b). On phases 1-3, the deflections have higher peaks by 20% due to the increase of the phase currents, while on phases 2-4 they have lower peaks and more harmonics. This also leads to the acceleration peak on phase 4 due to the couplings

(Fig. 17b). It is noted that the acceleration peaks of phases 1-3 are equal to those of the ATC but the acceleration peaks of phases 2-4 are reduced by 50% compared to the ATC. The acceleration energies, which evaluate the impact of the low frequency harmonics of the radial forces, are also reduced by 51% (local) and 54% (global) compared to the ATC.

In the direct sliding INC, there are still three phases excited during each electrical period, but these phases are regularly switched (Fig. 15c). Therefore, all four phases are periodically excited in an equal way. It is seen that the harmonic amplitudes of the radial forces in this case are significantly lower than those in both previous cases, however, some disturbance harmonics appear at low frequencies. As a result, the deflections and the acceleration are identical for all phases. The deflection peaks are reduced by 20% (Fig. 16c) and the acceleration peaks are reduced by 45% (Fig. 17c) compared to the ATC. As low frequency harmonics appear in radial forces, the acceleration energies are also investigated. They are reduced by 54% (local) and 59% (global) compared to the ATC, that means the low frequency harmonics do not bring negative impact on the accelerations.

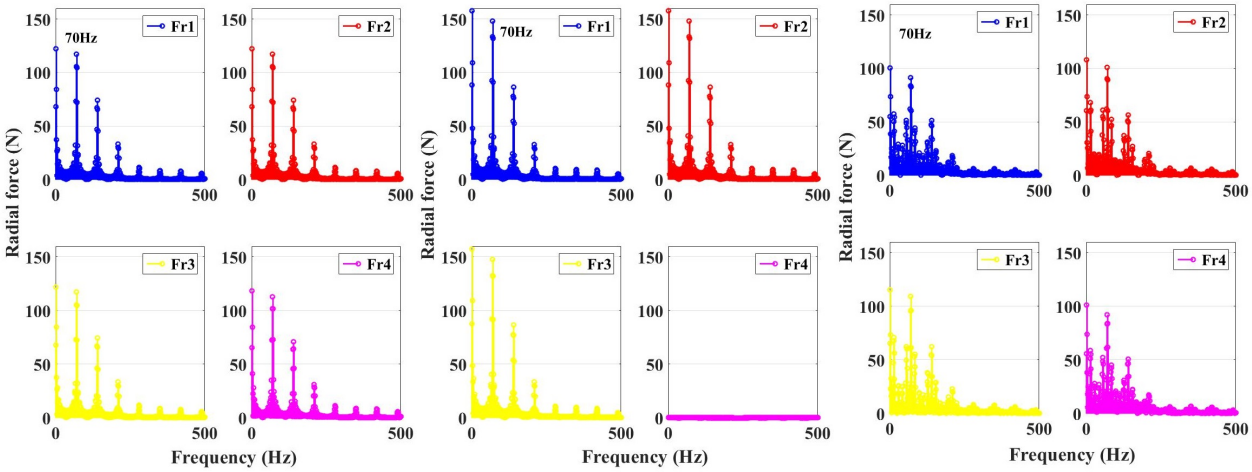

(a) ATC (b) Fixed INC (c) Direct sliding INC

Figure 15: Spectrums of the radial forces at $700rpm$, $6Nm$, $\alpha = 3/4$

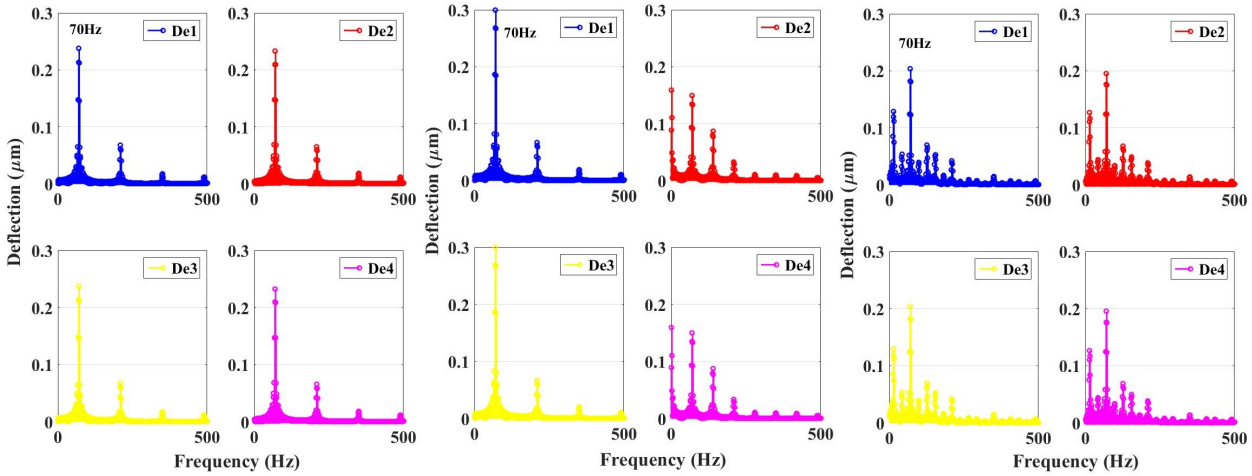

(a) ATC (b) Fixed INC (c) Direct sliding INC

Figure 16: Spectrums of the deflections at $700rpm$, $6Nm$, $\alpha = 3/4$

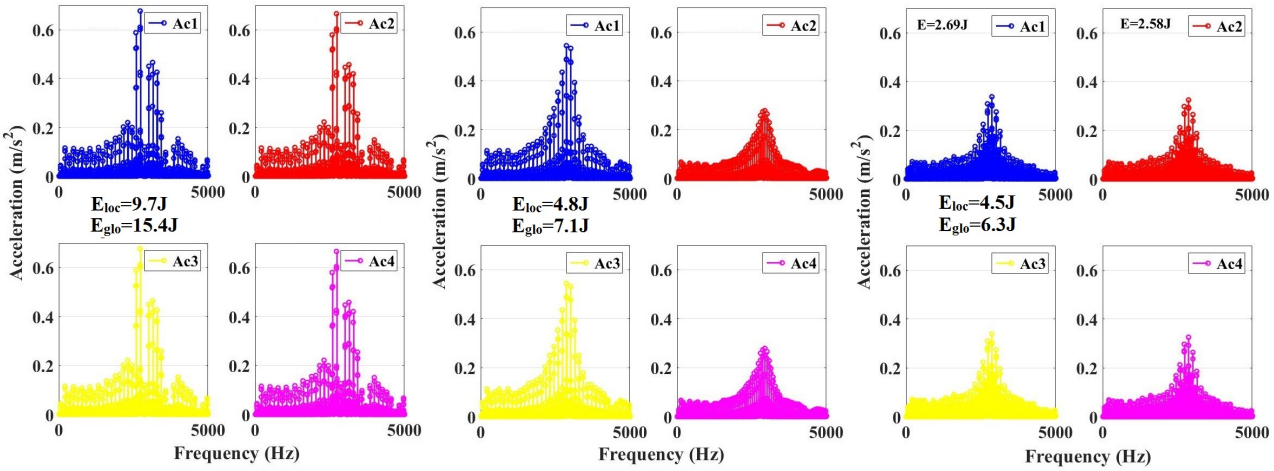

(a) ATC (b) Fixed INC (c) Direct sliding INC

Figure 17: Spectrums of the accelerations at $700rpm$, $6Nm$, $\alpha = 3/4$

For the operating point $700rpm$, $6Nm$, the INC reduces the vibration of the stator. More harmonics frequencies appear in the radial forces but the acceleration energies indicators show that they do not degrade the vibration.

4.2. SPECTRAL ANALYSIS OF DIFFERENT TORQUE-SPEED OPERATING ZONES

From Fig. 6, the vibratory impact of the INC needs to be verified on three torque-speed zones corresponding to three duty cycles on the entire speed range. As already seen in Fig. 15 to Fig. 17, changes in the radial forces lead to obvious changes in the deflection peaks (Fig. 18) and the acceleration peaks (Fig. 19), which are the first two vibration indicators. Moreover, as low frequency harmonics appear in the radial forces, the harmonics surrounding the resonance frequency rise in the accelerations. Therefore, two more indicators

which are the local spectral energy (Fig. 20) and the global spectral energy (Fig. 21) of the accelerations are investigated to evaluate the impact of the low frequency harmonics.

Fig. 18a (deflection peak), Fig. 19a (acceleration peak), Fig. 20a (local energy) and Fig. 21a (global energy) show the mapping results on zone (a) of the applicable zone of the INC with α=1/4 (Fig. 6). The fixed INC excites only phase 1 but its deflection and acceleration peaks appear on phases 1 and 3 due to the coupling between phases 1-3. The deflection peak is higher than that of the ATC due to the increase of the phase current. The acceleration peak is generally closed to that of the ATC. The local energy is higher than that of the ATC while the global energy is reduced. With the direct sliding INC, only one phase is supplied and regularly switched so the deflection and acceleration peaks appear in all phases. All indicators show that the direct sliding INC reduce the vibration in the zone a.

Fig. 18b (deflection peak), Fig. 19b (acceleration peak), Fig. 20b (local energy) and Fig. 21b (global energy) show the mapping results on zone (b) of the applicable zone of the INC with α=2/4 (Fig. 6). The fixed INC excites phases 1 and 2 but the deflection and acceleration peaks appears also on phases 2 and 4 due to the couplings. Generally, the deflection, the acceleration and the spectral energies are lower than those of the ATC except for the speed range from 2800rpm to 3600rpm. Besides, the direct sliding INC also reduces the deflection, the acceleration and the spectral energies. These results are even lower than those of the fixed INC, but from 2800rpm to 3600rpm it is still not better than the ATC. The reason is that with both INC strategies, the 10th harmonic of the radial forces at 2800rpm, and the 8th harmonic of the radial forces at 3600rpm (that equal the resonant frequency f2) have higher amplitude than those of the ATC, therefore, the INC increases the vibration.

Fig. 18c (deflection peak), Fig. 19c (acceleration peak), Fig. 20c (local energy) and Fig. 21c (global energy) show the mapping results on zone (c) of the applicable zone of the INC with α=2/4 (Fig. 6). The fixed INC excites phases 1, 2 and 3. The deflection and the acceleration speaks appear on all phases. Generally, the deflection peak, the acceleration peak and the spectral energies by the fixed INC are not better than those of the ATC. Besides, the direct sliding INC reduces these indicators. However, the differences between the controls are not significant because in the zone (c), the INC turns off only one phase and the reference torque is multiplied by only 4/3. In this case, both INC strategies increase the vibration in the speed range from 2800Hz to 3600Hz as explained previously.

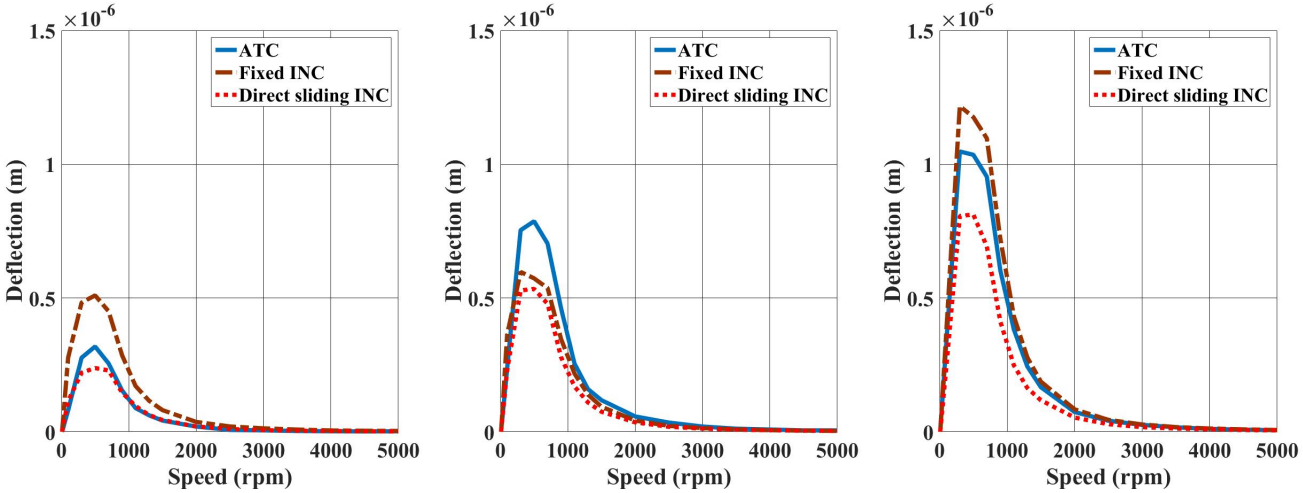

(a) Zone a α=1/4 (b) Zone b α=2/4 (c) Zone c α=3/4

Figure 18: Evolution of deflection peaks by three controls

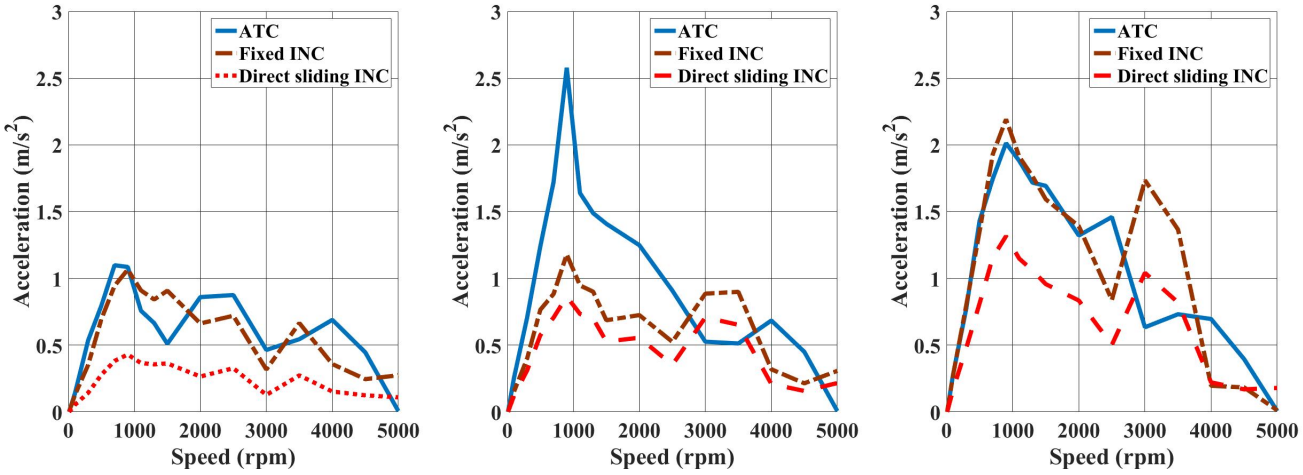

(a) Zone a α=1/4 (b) Zone b α=2/4 (c) Zone c α=3/4

Figure 19: Evolution of acceleration peaks by three controls

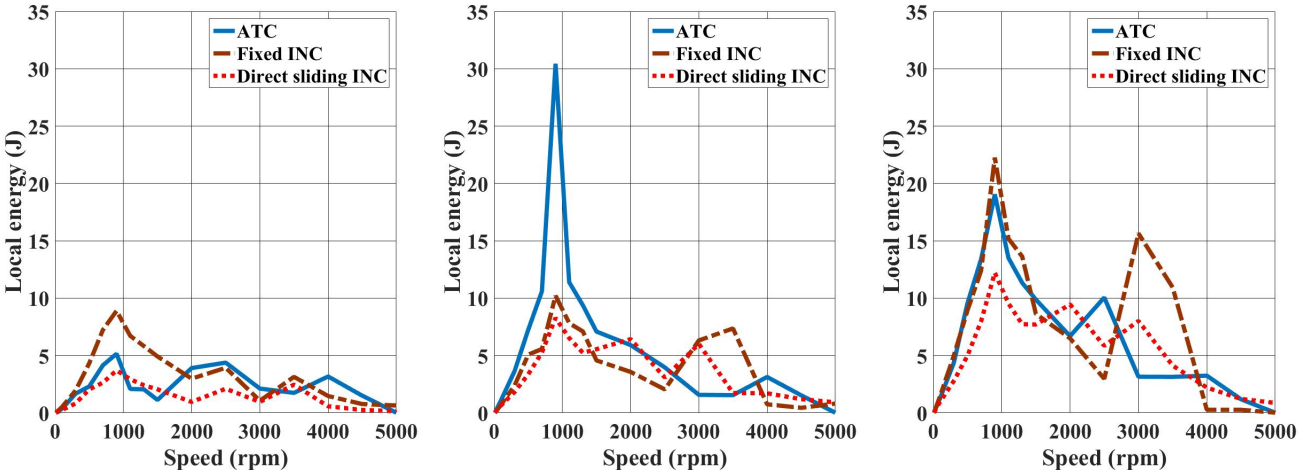

(a) Zone a α=1/4 (b) Zone b α=2/4 (c) Zone c α=3/4

Figure 20: Evolution of acceleration local energies by three controls

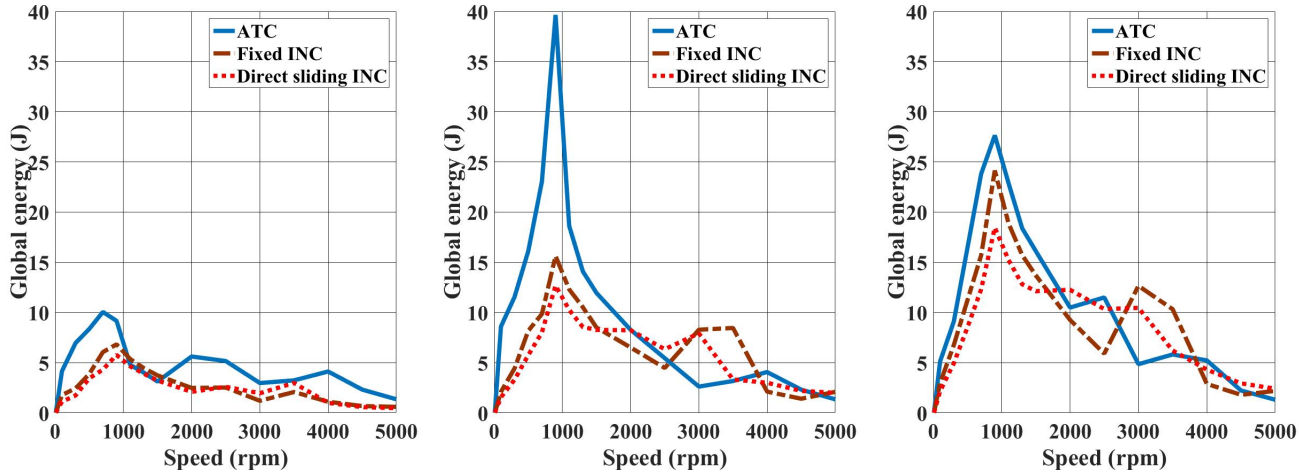

(a) Zone a α=1/4 (b) Zone b α=2/4 (c) Zone c α=3/4

Figure 21: Evolution of acceleration global energies by three controls

In simulation, the INC excites more low frequency harmonics in the radial forces. The spectral energy analysis shows that they do not bring unexpected impact the the vibration. Especially, the direct sliding INC can reduce the vibration while it reduces the losses. However, at certain speeds it tends to excite the mode 2 and probably other modes of the SRM that need to verify experimentally.

5. EXPERIMENTAL VALIDATION

This section presents the test bench and the experimental results that validate the simulation results. In experimentation, not only vibration mode 2 but the other modes of the

SRM which are within the audible zone of human are also illustrated which permit to globally evaluate the INC. The experimental validation has been achieved with the test bench shown in Fig. 22.

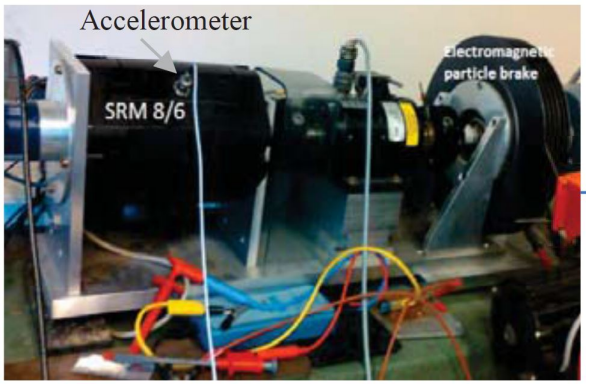

Figure 22: Test bench

The test bench consists of three elements: the electromechanical system, the control unit and the measurement. The system comprises the converter and the SRM fed by a DC supplier and coupled with a controlled torque load which permit to adjust the resistant torque. The control unit is based on a digital control processor dSPACE equipped with FPGA. In fact, the speed and torque regulation is performed by the processor while the current regulation is performed by the fast FPGA to assure the rapid computational time. The measurement consists of voltage probes, current sensors, an encoder to measure the rotor angular position/speed, a torque sensor to measure the torque on shaft and an accelerometer to measure the actual accelerations of the SRM.

Fig. 23 show the accelerations given by three controls at $700rpm$, $2Nm$, $\alpha = 1/4$. The mode 2 is reduced by the fixed strategy and the direct sliding strategy as already seen in the simulation. The other modes ($12kHz$, $14kHz$) are also reduced by both INC strategies. Considering the acceleration energy, the fixed strategy increases this value because the harmonics are more important (dark blue) while the direct sliding strategy reduces the energy.

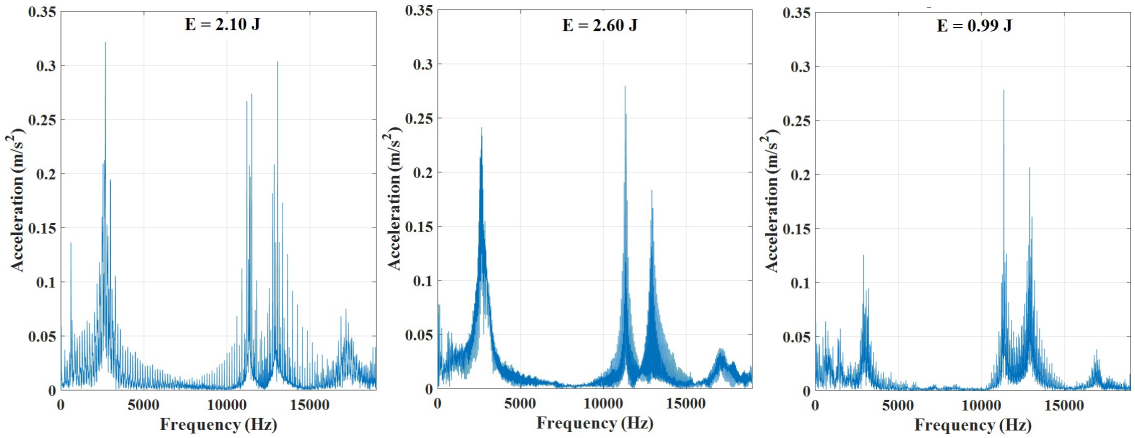

(a) ATC (b) Fixed INC (c) Direct sliding INC

Figure 23: Spectrums of the accelerations at $700rpm$, $2Nm$, $\alpha = 1/4$

Fig. 24 show the accelerations given by three controls at $700rpm$, $4Nm$, $\alpha = 2/4$. Mode 2 is reduced by the fixed and the direct sliding strategies as also seen in the simulation. However, the fixed strategy increases the mode 4 while the direct sliding strategy reduces all modes. With the acceleration energy, the direct sliding strategy also gives lower value.

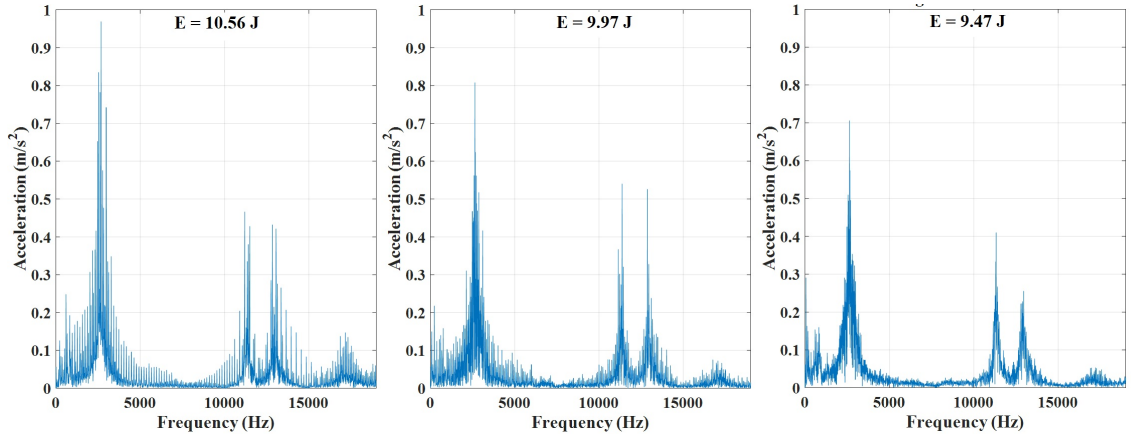

(a) ATC (b) Fixed INC (c) Direct sliding INC

Figure 24: Spectrums of the accelerations at $700rpm$, $4Nm$, $\alpha = 2/4$

Fig. 25 shows the accelerations given by three controls at $700rpm$, $6Nm$, $\alpha = 3/4$. Which is the same operating point analyzed in simulation. This case is quiet regular when both INC strategies reduces the vibration in terms of acceleration peak and acceleration energy. Therefore, the direct sliding strategy proves to be the good one to reduce the vibration.

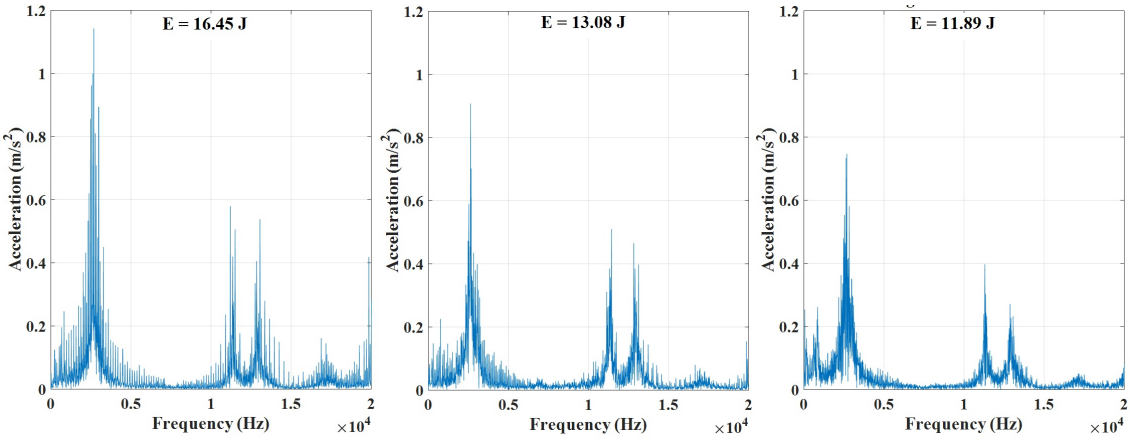

(a) ATC (b) Fixed INC (c) Direct sliding INC

Figure 25: Spectrums of the accelerations at $700rpm$, $6Nm$, $\alpha = 3/4$

In addition, the fact that only some fixed phases are supplied by the fixed strategy can overheat these phases that leads to the degradation of the windings and the demand of cooling effort. In contrast, the direct sliding strategy switches regularly the supplied phases that leads to not only the equal temperature distribution but also vibration reduction.

6. CONCLUSION

This paper presents the INC for the purpose of increasing the global efficiency of the SRM and the converter in automotive applications. However, stator vibration is an important drawback of the SRM which can cause acoustic noise. Therefore, the vibratory impact of different INC strategies is studied and analyzed using a simplified vibratory model.

Authors use a simplified vibratory model for mode 2 which allows to evaluate rapidly the vibratory impact of the controls on the entire torque-speed plane. The obtained simulation results show that the direct sliding INC distributes equally the radial forces and the total accelerations on all phases and hence reduces generally the vibratory impact on mode 2 compared to the ATC. The experimental results validate that the direct sliding INC reduces or at least does not degrade the other modes of the SRM.

The direct sliding INC is also preferred when considering the operation temperature as it switched regularly the phases. Along with the efficiency the machine vibration criteria, the impact of the INC on the torque pulsation, the vehicle dynamic is also studied in [21]. From all these criteria, a final strategy of the INC are being built and tested on common driving cycles.

References

[1] C. C. Chan, "The State of the Art of Electric, Hybrid, and Fuel Cell Vehicles," in Proceedings of the IEEE, vol. 95, no. 4, pp. 704-718, April 2007.

[2] K. M. Rahman, B. Fahimi, G. Suresh, A. V. Rajarathnam and M. Ehsani, "Advantages of switched reluctance motor applications to EV and HEV: design and control issues,"

in IEEE Transactions on Industry Applications, vol. 36, no. 1, pp. 111-121, Jan/Feb 2000.

[3] V. Raulin, A. Radun and I. Husain, "Modeling of losses in switched reluctance machines," in IEEE Transactions on Industry Applications, vol. 40, no. 6, pp. 1560-1569, Nov.-Dec. 2004.

[4] S. D. Calverley, G. W. Jewell and R. J. Saunders, "Prediction and measurement of core losses in a high-speed switched-reluctance Machine," in IEEE Transactions on Magnetics, vol. 41, no. 11, pp. 4288-4298, Nov. 2005.

[5] B. Ganji, Z. Mansourkiaee, J. Faiz, "A fast general core loss model for switched reluctance machine", In Energy, Volume 89, 2015, Pages 100-105, ISSN 0360-5442, https://doi.org/10.1016/j.energy.2015.07.058.

[6] C. Mademlis and I. Kioskeridis, "Performance optimization in switched reluctance motor drives with online commutation angle control," in IEEE Transactions on Energy Conversion, vol. 18, no. 3, pp. 448-457, Sept. 2003.

[7] I. Ralev, F. Qi, B. Burkhart, A. Klein-Hessling and R. W. De Doncker, "Impact of smooth torque control on the efficiency of a high-speed automotive SRM drive," 2016 IEEE International Power Electronics and Motion Control Conference (PEMC), pp. 580-585, Varna, 2016.

[8] D. M. Nguyen, I. Bahri, G. Krebs and C. Marchand, "Intermittent control for efficiency gain of a switched reluctance machine," 2017 IEEE International Electric Machines and Drives Conference (IEMDC), Miami, FL, 2017, pp. 1-7.

[9] F. Roy, A. M. Catania, F. Ossart and C. Marchand, "Hybrid powertrain design using optimal control strategies," Electric Vehicle Symposium and Exhibition (EVS27), 2013 World, pp. 1-7, Barcelona, 2013.

[10] Pierre Millithaler, Jean-Baptiste Dupont, Morvan Ouisse, Émeline Sadoulet-Reboul, Noureddine Bouhaddi, "Viscoelastic property tuning for reducing noise radiated by switched-reluctance machines", In Journal of Sound and Vibration, Volume 407, 2017, Pages 191-208, ISSN 0022-460X, https://doi.org/10.1016/j.jsv.2017.07.008.

[11] Yanyang Wang, Pingfei Li, Guizhou Ren, "Electric vehicles with in-wheel switched reluctance motors: Coupling effects between road excitation and the unbalanced radial force", In Journal of Sound and Vibration, Volume 372, 2016, Pages 69-81, ISSN 0022-460X, https://doi.org/10.1016/j.jsv.2016.02.040.

[12] F. C. Lin and S. M. Yang, "Instantaneous Shaft Radial Force Control with Sinusoidal Excitations for Switched Reluctance Motors," in IEEE Transactions on Energy Conversion, vol. 22, no. 3, pp. 629-636, Sept. 2007.

[13] A. Klein-Hessling, A. Hofmann and R. W. De Doncker, "Direct instantaneous torque and force control: a control approach for switched reluctance machines," in IET Electric Power Applications, vol. 11, no. 5, pp. 935-943, 5 2017.

[14] M. Boesing, A. Hofmann and R. De Doncker, "Universal acoustic modelling framework for electrical drives," in IET Power Electronics, vol. 8, no. 5, pp. 693-699, 5 2015.

[15] F. L. M. dos Santos, J. Anthonis, F. Naclerio, J. J. C. Gyselinck, H. Van der Auweraer and L. C. S. Góes, "Multiphysics NVH Modeling: Simulation of a Switched Reluctance Motor for an Electric Vehicle," in IEEE Transactions on Industrial Electronics, vol. 61, no. 1, pp. 469-476, Jan. 2014.

[16] I. Bahri, H. Maamri, E. Berthelot, E. Godoy and C. Marchand, "Comparison of two control strategies regarding vibration criterion for switched reluctance machine," 8th IET International Conference on Power Electronics, Machines and Drives (PEMD 2016), Glasgow 2016, pp. 1-6.

[17] D. M. Nguyen, I. Bahri, G. Krebs and C. Marchand, "Impact of the intermittent control on the vibration behavior of a switched reluctance machine," 2017 Electrimacs Conference, Toulouse, 2017.

[18] H. Hannoun, M. Hilairet and C. Marchand, "Design of an SRM Speed Control Strategy for a Wide Range of Operating Speeds," in IEEE Transactions on Industrial Electronics, vol. 57, no. 9, pp. 2911-2921, Sept. 2010.

[19] Muhammad Usman Jamil, Waree Kongprawechnon, Nattapon Chayopitak, "Average Torque Control of a Switched Reluctance Motor Drive for Light Electric Vehicle Applications", In IFAC-PapersOnLine, Volume 50, Issue 1, 2017, Pages 11535-11540, ISSN 2405-8963, https://doi.org/10.1016/j.ifacol.2017.08.1628.

[20] M. Rekik, M. Besbes, C. Marchand, B. Multon, S. Loudot, D. Lhotellier, "Optimisation du nombre de spires et des angles de commande d'un moteur à réluctance variable à double saillance pour application de traction électrique", Electrotechnique du Futur, Grenoble, 2005.

[21] D. M. Nguyen, I. Bahri, G. Krebs and C. Marchand, "Impact of the intermittent control on the torque pulsation of a switched reluctance machine," 2017 IEEE Vehicle Power and Propulsion Conference (VPPC), Belfort, 2017. (presented)

[22] M. Besbes, B. Multon, "MRVSim code: Logiciel de simulation pour l'aide au dimensionnement des MRVDS et des convertisseurs", Patent, N: IDDN. FR. 001. 430010. 000. S. C. 2004. 000. 30645, 2004.

[23] J. O. Fiedler, K. A. Kasper and R. W. De Doncker, "Calculation of the Acoustic Noise Spectrum of SRM Using Modal Superposition," in IEEE Transactions on Industrial Electronics, vol. 57, no. 9, pp. 2939-2945, Sept. 2010.

[24] Rasmussen, F. Blaabjerg, J. Pedersen, P. Kjaer, and T. Miller, "Acoustic noise simulation for switched reluctance motors with audible output," in Proc. Eur. Conf. Power Electron. Appl. (EPE), (1999).

[25] M. Belhadi, G. Krebs, C. Marchand, H. Hannoun and X. Mininger, "Evaluation of a switched reluctance motor with magnetic slot wedges," 2014 International Conference on Electrical Machines (ICEM), Berlin, 2014, pp. 150-155.

[26] D. M. Nguyen, I. Bahri, G. Krebs and C. Marchand, "Performance of the intermittent control for switched reluctance machine on driving cycle," 2018 IEEE International Conference on Electric Machines (ICEM), Alexandroupoli, 2018. (submitted)